Full wave front reconstruction in the Fourier domain

E. N. Ribak[a], Y. Carmon[a], A. Talmi[b], O. Glazer[a], O. Srour[a] and N. Zon[a]
[a]Technion – Israel Institute of Technology, Haifa 32000, Israel;
[b]Timi Technologies Ltd., Ramat Hashofet 19238, Israel

ABSTRACT

Recently we developed and tested different algorithms for wave front reconstruction from dense Hartmann-Shack patterns. All depend on the recognition of a main frequency in the patterns, whose distortion from wave aberrations can be construed as slight phase changes in the pattern. An alternative description of these aberrations is a slight frequency change in Fourier domain. The slopes can thus be found by demodulation in either the image or the Fourier domain. These slopes can then be integrated in the Fourier domain again for the wave front itself. For smooth slopes both demodulation and integration can be performed in the Fourier domain. In addition, commands for the adaptive optics loop can be taken directly in the Fourier domain, saving on processing time. We modeled and tested these algorithms thoroughly in simulation and in laboratory experiments on two separate adaptive optics systems.

Keywords: adaptive optics, Fourier demodulation, Hartmann-Shack wave front sensor, adaptive optics control

1. INTRODUCTION

Hartmann-Shack (HS) wave front sensors are very common in the fields of wave front sensing for controlling adaptive optics systems. These tasks are rather similar, but only in some cases. For simple adaptive optics systems, where the number of lenslets is low, it is possible to deduce directly from the movements of the HS centroids what are the commands for the deformable mirrors. However, in cases where the number of lenslets is very large, such as in big telescopes at shorter wave lengths, it seems that centroids calculation is not the most efficient method. This is also true in other cases in adaptive optics (for example, ocular and laser correction) where light is abundant and the wave front can also be sampled with many lenslets.

There are two traditional descriptions of wave fronts, zonal and modal. In the zonal method the value of the wave front is described in Cartesian coordinates, $W(x, y)$. If one wishes to use modes of a mirror whose actuators are on a Cartesian grid, or after passage through turbulence with a Kolmogorov (or fractal) spectrum, then the wave front will be described along these modes, $W[\mathrm{K}(x, y)]$. Alternatively, the description of the wave front itself in polar coordinates, $W(\rho, \theta)$, or on the round aperture or mirror modes is possible, $W[\mathrm{Z}(\rho, \theta)]$. The Cartesian cases are very convenient for Fourier description, as either the wave front itself or its gradient can be described in few Fourier components.

Following this line, initiated by Roddier[1], we developed a number of methods to (a) calculate the wave front slopes from the HS pattern, (b) calculate the wave front itself from its slopes, (c) calculate the control commands directly in the Fourier domain, and (d) calculate the wave front itself from the HS in the Fourier domain. We also analyzed the noise behavior of these methods.

2. Fourier analysis

It is quite easy to understand the idea behind these methods if one considers the HS pattern as a grid of δ functions whose transform is

$$I_0(x, y) = \sum_{m,n=0}^{\infty} a_{m,n} \left(\cos 2\pi m x / P + \cos 2\pi n y / P \right). \tag{1}$$

The grid period, or the lenslet pitch, is $P = 2\pi / k$. We neglect all high harmonics, and concentrate on the lowest one,

$$I_0(x, y) \approx \cos kx + \cos ky. \tag{2}$$

The higher harmonics ignored actually describe the shape of the spots, which for simplicity we assume is constant. When the wave front is not flat, these waves will be shifted locally by $F\nabla W$, thus

$$I(x, y) \approx \cos(kx + FW_x) + \cos(ky + FW_y), \tag{3}$$

where W_x and W_y are the gradient components. Writing the cosines as sums of exponentials and transforming, one gets

$$\bar{I}(u,v) \approx \overline{e^{-iFW_x}} * \delta(u-k) + \overline{e^{iFW_x}} * \delta(u+k) + \overline{e^{-iFW_y}} * \delta(v-k) + \overline{e^{iFW_y}} * \delta(v+k), \tag{4}$$

where $\bar{I}$ or signifies a Fourier transform of I, etc. Thus we see that each side lobe, at distance k from the Fourier origin, carries the Fourier transform of the wave front slope.

2.1. Simple demodulation

From Eq. 4 it is clear that to get the gradient, all one has to do is take the vicinity of each side lobe, down-shift it to the origin, and inverse-transform it to the image domain, to get exp $\pm iFW_x$ and exp $\pm iFW_x$ (Fig. 1). The arguments of these two quantities are the sought slopes[2] FW_x., FW_y. Care should be taken to avoid aliasing in the first Fourier transform, e.g. by employing a empty array of double the size, into which the HS pattern is copied before the transform (zero padding).

The vicinity of the side lobe, that which is defined by the width of the low-pass filter, is at maximum within one-half the frequency k. Usually, it is much smaller, and can be defined as the known number of degrees of freedom of the detector. It is also akin to limiting the collimation of the beam (usually performed by a mechanical filter in the focal plane), as it rejects high-frequency noise on the side lobes. This noise is masquerading as additive noise on the wave front slope components.

It should be pointed out that since only very few Fourier components might be necessary, it might be easier to perform a digital Fourier transform, rather than a fast Fourier transform. The latter calculates the values at all Fourier frequencies, while we might need only the ones near the orthogonal side lobes (the first and third terms in Eq. 4). However, since we are now calculating very few frequencies, perhaps we should switch to only the main one, as the next section shows.

2.2. Convolution

The process of Fourier demodulation can also be performed without reverting to Fourier transforms. There are two stages in the demodulation in the Fourier domain: down-shifting in frequency, and taking only the vicinity of each side lobe. These two stages have image-plane equivalents: shifting in frequency, say by k in the x direction, is equivalent to multiplying the HS pattern by exp $-ikx$. Then choosing the neighbourhood of the side lobe near the Fourier origin is equivalent to smoothing or low-pass filtering of the image[3]. The filter kernel is of the size of the lenslet pitch P.

Thus the procedure is rather simple: multiply the HS pattern by exp $-ikx$, and then run a smoothing convolution on the resultant complex image. Finally, take the argument of the result, to get FW_x. Then repeat the procedure in the orthogonal direction, by multiplying by exp $-iky$, smoothing, and finally taking the argument to get FW_y.

2.3. Smoothing

We have seen the time saving in going from demodulation to deconvolution: instead of one direct and two inverse Fourier transforms, two convolutions are performed. If the lenslet pitch P is small compared to the array size, this is indeed significant. However, more saving in time is possible if one employs another smoothing scheme[3]. The method we have used was a simple shift-and-add scheme: if the smoothing kernel is, say, 1, 2, 1, then by shifting the array by half the pitch and adding double that array to the original array would achieve this fit (notice that due to the multiplication before by exp $-ikx$, all arrays are now complex). Similarly, if the smoothing kernel is 1, 2, 4, 2, 1, we need to repeat the previous procedure again, now at one-quarter the pitch. A finer, and less noisy, result is achieved by again halving the shift-and-add period. These smoothing steps are performed first in one direction, then in the orthogonal one. Finally, the argument is extracted to yield one wave front gradient component. Then it is repeated for the second gradient component.

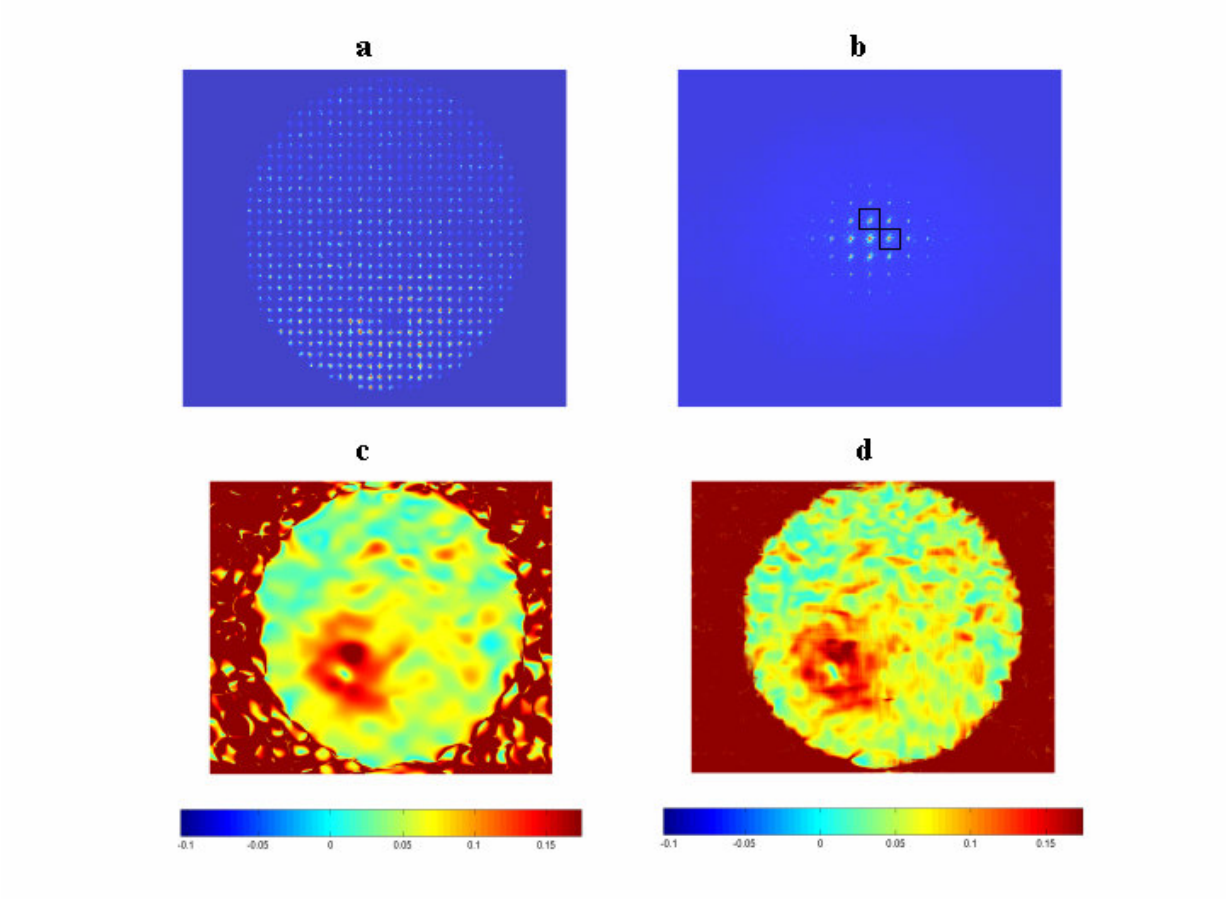

Fig. 1. Demodulation of a Hartmann-Shack pattern, showing the response of a deformable mirror to the poking of one element. (a) grid of spots; (b) Fourier transform of (a) showing the x and y side lobes; (c) $|\nabla W(x,y)|$, calculated by smoothing (a); (d) $|\nabla W(x,y)|$, calculated by Fourier demodulation of (b). The box size in (b) or the kernel in (c) set the smoothness of the results.

2.4. Borderline cases

Typically we have an edge to the HS pattern, usually a round aperture and most times also a central obscuration. These edges might mean including in the slopes terms from outside the pupil. While this might reduce the quality of the results near the edge, it might have strong repercussions when integrating the slopes into the wave front itself: the boundary conditions influence the whole result, as is usual in solving partial differential equations, and noisy conditions might destroy it. A solution to this problem was found by assuming that the slope is constant at the edges, or that a closed integral which includes the boundary is zero. We were able to achieve this by duplicating the last HS spots exactly one period P outside the aperture.

To perform the duplication beyond the edge, we copied the array, shifted by $\pm P$, to the four sides of the original array (an alternative is shifting at $\pm 45^0$). The four shifted and added images were replaced in the center by the original array. Notice that if the pitch is not exactly an integer number of pixels, secondary errors might occur, in which case an interpolated shift might be necessary.

2.5. signal to noise ratio

It is interesting to compare the centroids analysis method to the Fourier analysis method in terms of photon and digitization noise[9]. For bright objects, the Fourier method performs much better. This is because pixelization plays a significant role in centroiding. Errors, stemming from a shift of the centroid outside its designated area, bias its location. In Fourier methods the shift of the pattern as a whole is examined, so this error does not exist.

Centroiding, for an infinite number of pixels per spot, is equivalent to Fourier analysis for any number of pixels per spot (Fig. 2). Only large read out noise can offset this advantage of a large number of pixels (more pixels mean more distant Fourier side lobes and hence easier separation and low-pass filtering).

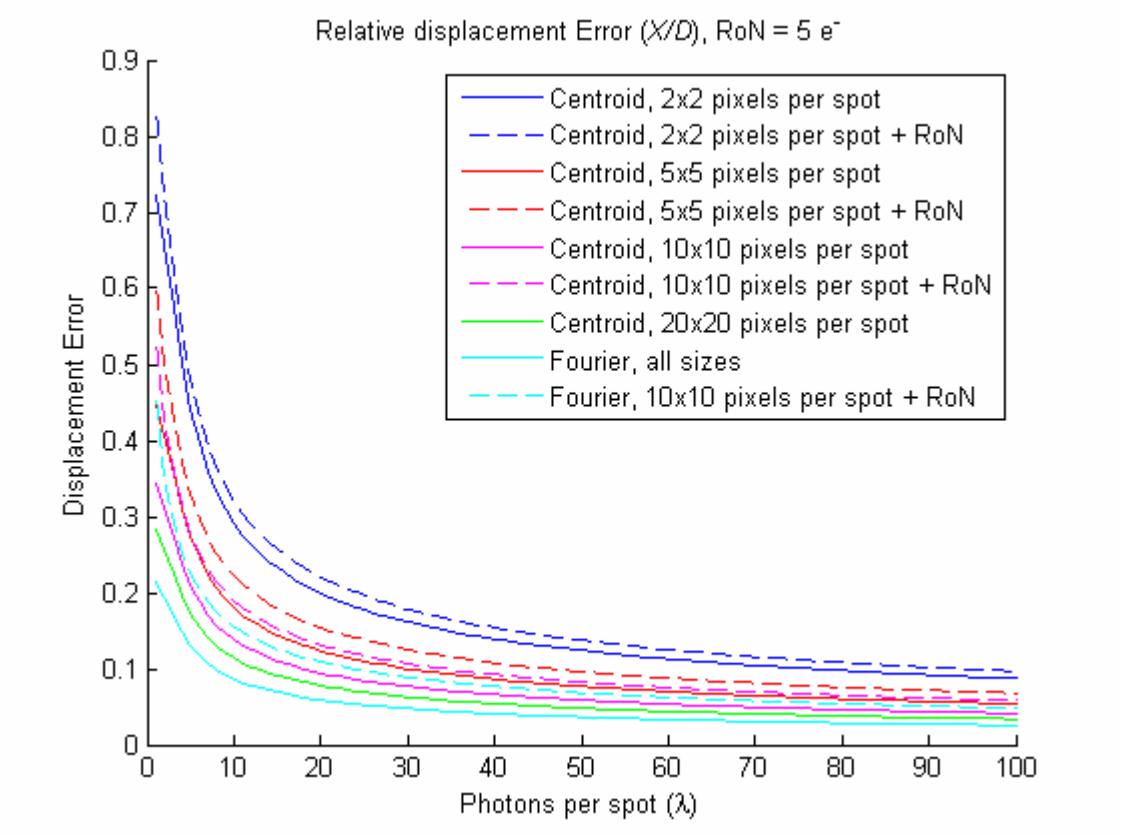

Fig. 2. Comparison of the relative error in the centroids' positions, for different box sizes. Pixelization adds to the uncertainly in small sub-arrays (but not in the Fourier method) while read out noise contributes only in large arrays.

3. Fourier control

It is customary to use the *x* and *y* slopes of the wave front as an input to the reconstructor matrix. This matrix is the inverse of the interaction matrix, created by moving each deformable mirror element at a time. The slopes resulting from each poke are lined up along each corresponding matrix column. Singular value decomposition or other pseudo-inverse of that interaction matrix will create the reconstructor matrix. In the Fourier scheme this is performed in either one of two ways, corresponding to the chosen process:

3.1. Side lobes

As the complex values around each side lobe frequency describe the components of the transform in full, they are equivalent to the values of the slopes as described in Section 2.1 (Fig. 3). Hence, it is possible to take these values as inputs for the interaction matrix (Fig. 4). Notice that the transform values are complex, but only their anti-hermitian part carries the information[4] (see section 4.1). We have also found experimentally that the imaginary part can be sufficient[5]. The major convenience stems from the knowledge that usually only the lowest Fourier modes are necessary to describe the common wave front perturbations, as well as modes of the deformable mirror. As in the image domain, this can be verified by employing single value decomposition of the data and finding the most important modes in the Fourier domain. Another convenience is the fact that only one Fourier transform is necessary, without any centroiding (for the terse detection scheme of four pixels per spot, the two are nearly equivalent).

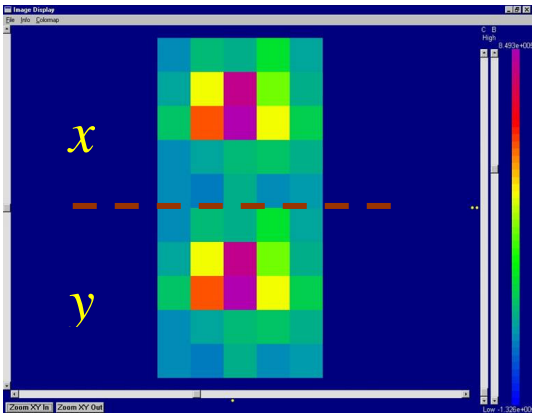

Fig. 3. Screenshot of the imaginary part of the two side lobes used as an input to the adaptive optics loop (after staggering to one line).

3.2. Sampled wave front

If no Fourier transform is carried out, the result of convolution or smoothing is two frames holding the two components of the wave front slope (Sections 2.2 or 2.3). The resolution is the same as the detector resolution, not the HS pitch resolution (Fig. 5). This means that the resultant wave front is over-sampled, with many redundant pixels, but without the higher frequency noise. The big advantage is that for the first time it is possible to optimize the locations at which the wave front slopes are sampled for the reconstructor, regularly or at a density which varies across the aperture and mirror. Previously, one had to locate the lenslets judiciously at these locations, limited by the constraint of lenslet size and other hardware constraints. Moreover, there is no need to choose any more whether the Fried or Hudgin scheme is preferable.

We have indeed constructed such a control system, where the control commands are taken from few pixels inside the wave front slopes[4]. The loop was very successful in correcting variable wave front aberrations in the lab.

4. wave front reconstruction

For diagnostic applications, for piston deformable mirrors, and for non-astronomical applications it is necessary to construct the wave front itself from its slopes. The first solutions were given in the image domain, and were based on least-squares fitting of the wave front to the given slopes. Later solutions for the problem employed direct or least squares fitting of the data in the Fourier domain. Given the slopes W_x and Wy, it is possible to show that the wave front is given by

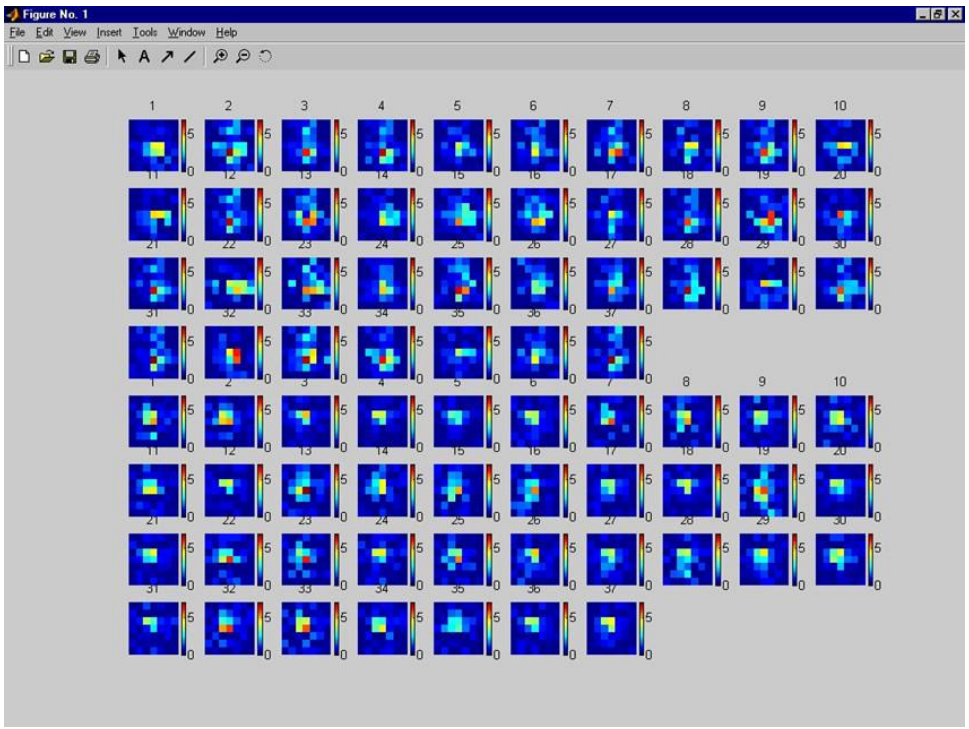

Fig. 4. To construct the interaction matrix in the Fourier domain, each of the 37 electrodes was poked, and the 25+25 pixels describing the two gradient transforms were used. Here we show all the transforms of all the responses, *x* at the top and *y* at the bottom.

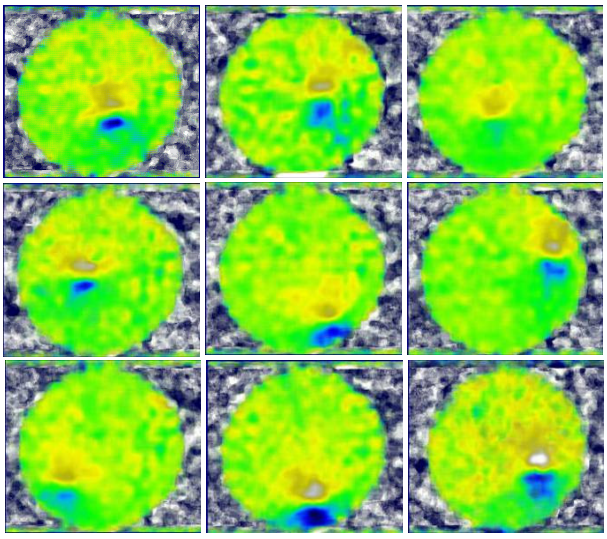

Fig. 5. To construct the same matrix in the image plane, each of the 37 electrodes was poked, and the result smoothed (showing only the *y* slope of 9 elements). For the matrix, 25 points were sampled within the aperture.

$$\overline{W}(u,v)=\frac{u\overline{W_x}(u,v)+v\overline{W_y}(u,v)}{u^2+v^2}, \tag{5}$$

and the boundary conditions, on a round aperture, are imposed iteratively[5]. On a rectangular aperture the solution is

$$\overline{W}(u,v)=\frac{\sin u\,\overline{W_x}(u,v)+\sin v\,\overline{W_y}(u,v)}{\sin^2 u+\sin^2 v}, \tag{6}$$

based on a least squares solution[6]. It is not easy to use this solution on other pupil shapes, and it suffers from its inability to take care of slope errors, because of the repeatability of the discrete Fourier transform. We were able to propose a different solution using sine and cosine transforms[7], of the shape

$$\overline{W}(u,v)=\frac{T(u)\,\overline{S_x}(u,v)+T(v)\,\overline{S_y}(u,v)}{T^2(u)+T^2(v)}, \tag{7}$$

where $T(z) = 2 \sin(z/2)$. The slope transforms are also given by the sine and cosine transforms[7]. This method employs only the lower half of the frequency range and also results in a lower variance. Using fast diagonal multi-grid methods for the solution[7], the wave front can be solved over any pupil, including those with central obscuration.

4.1. Fourier full reconstruction

When the wave front is ergodic, namely the slopes are well-behaved and not too high, it is possible to perform both demodulation and integration in the Fourier domain[8]. Until now, these two stages were separate. First the pattern was transformed, shifted and transformed back twice, to yield the phase function of the wave front (Section 2.1). After calculation of the arguments, both slopes were transformed back into the Fourier domain, and the integration was carried out (Eqs. 5, 6, or 7). Then the result was transformed back to yield the final wave front. This required six transforms, slowing the process significantly. Starting from centroiding, Fourier integration required three transforms.

If the wave front fluctuations are indeed small, the phase $\varphi = \varphi(x, y)$ can be written as a Taylor series. Let the amplitude through the pupil be $A = A(x, y) \approx A_0 + \delta A$, with a mean value A_0 and perturbation (scintillation) δA. The approximated wave will be

$$R = A\exp(i\varphi) \approx A\left[\left(\varphi-\tfrac{1}{6}\varphi^3\right)+i\left(1-\tfrac{1}{2}\varphi^2\right)\right]. \tag{8}$$

Separating the hermitian and anti-hermitian parts of the Fourier transform of R we get

$$\overline{\varphi}=\frac{\overline{R}-\overline{R}^*}{2A_0};\ \overline{A_0}=\frac{\overline{R}+\overline{R}^*}{2}, \tag{9}$$

where $\overline{R}^*$ is the complex conjugate of $\overline{R}$, which in turn is the Fourier transform of R. Eq. 9 shows that while once are at the Fourier domain, we can take the anti-hermitian part of the transform, and obtain the two components of the wave front slope. In one case we get $\overline{W_x}$ from one side lobe of the transform, and similarly $\overline{W_y}$ from the other side lobe. These two are to be plugged in either of Eqs. 5, 6, or 7, and transformed back to yield the wave front itself. We see that the process includes one Fourier transform, calculation of the anti-hermitian parts, division (for integration) and a second, inverse Fourier transform. The signal to noise ratio of this method is comparable to the other methods, and the processing time is much shorter[8]. Another advantage is the fact that the slopes never need to be unwrapped. This step can sometimes bring about phase jumps, which are not tolerable. Performing the whole process in the Fourier domain, this problem is circumvented. The results are comparable to the other methods (Fig. 6).

5. multi-conjugate adaptive optics

Fourier methods also have their place in detection of aberrations in a few layers in the atmosphere. Some schemes rely on shearing interferometers[10, 11] or pyramid arrays[12] to analyze projected fringes or spot arrays in the sky or on their Fourier analysis[13]. Fourier methods have also been successful in solar multi-conjugate adaptive optics[14] and so it might be possible to follow that example: by placing two wave front sensors conjugate to two turbulent layers, and Fourier analyzing each, one should get information about the two layers[15]. Even if each lenslet now views many stars in its field of view, the transform of the whole constellation is affected by the layer turbulence only. In other words, the addition of more stars only adds to the signal at the designated side lobe[10, 11] as can be seen in Fig. 7.

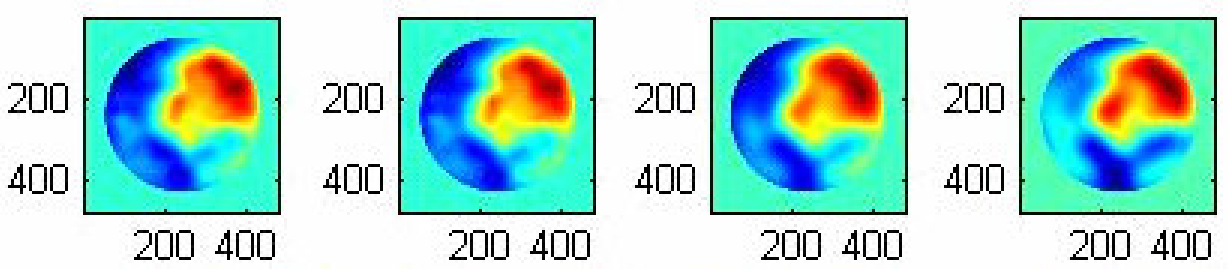

Fig. 6. Analysis of the same Hartmann-Shack pattern in four methods (from left) convolution, smoothing, Fourier, and fast Fourier. The constant of (double) integration in the Fourier methods can be different from the image plane methods.

Surprisingly enough, when the telescope is large (and how large is not quantified yet), it might be possible to use natural star light, from all stars in the field of view, to separate the atmospheric layers. The main draw back of this method is the number of pixels necessary to sense the wave fronts: it is as large as the size of a camera observing the same astronomical field, with pixels matching the diffraction limit of the telescope[15]. The camera might have to be a mosaic of smaller cameras, but each camera needs to read only the stars and ignore the empty areas in between, to reduce read time and noise.

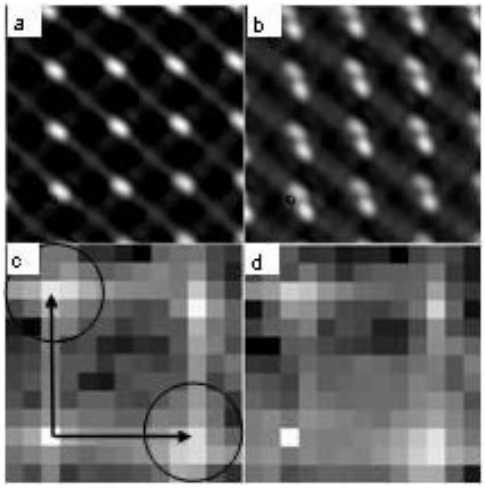

Fig. 7. One and two pinholes represent Hartmann-Shack patterns from one (a) or two stars (b). The measurements are transformed (c, d) but the side lobes (circled) remain essentially the same, yielding the average wave front over the aperture. During observation, only the pixels where stars appear are read out, saving in time and in noise.

Acknowledgments: Parts of this work were conducted within the Extremely Large Telescope Design Study, which is a technology development program funded by the European Community under contract No 011863. Sharp-Eye, a European Research and Training Network supported Carmen Canovas-Vidal, who helped with the comparison between the different methods.

REFERENCES

1. F. Roddier, *Adaptive Optics in Astronomy*, Cambridge University Press, 1999.
2. Y. Carmon and E. N. Ribak, "Phase retrieval by demodulation of a Hartmann-Shack sensor", *Opt. Comm.* **215,** 285 - 288 (2003).
3. A. Talmi and E. N. Ribak, "Direct demodulation of Hartmann-Shack patterns", *J. Opt. Soc. Am. A* **21,** 632-9 (2004).
4. O. Glazer, E. N. Ribak and L. Mirkin, "Adaptive optics implementation with a Fourier reconstructor", subm. (2006).
5. F. Roddier and C. Roddier, "Wavefront reconstruction using iterative Fourier transforms," *Appl. Opt*. **30**, 1325–1327 (1991).
6. K. R. Freischlad and C. L. Koliopoulos, "Modal estimation of a wave front from difference measurements using the discrete Fourier transform," *J. Opt. Soc. Am. A* **3**, 1852–1861 (1986).
7. A. Talmi and E. N. Ribak, "Wavefront reconstruction from its gradients". *J. Opt. Soc. Am. A* **23,** 288-297 (2006).
8. Y. Carmon and E. N. Ribak, "Fast Fourier demodulation", *Appl. Phys. Lett.* **84,** 4656-4567 (2004).
9. N. Zon, O. Srour, and E. N. Ribak, "Hartmann-Shack analysis errors". *Optics Express* **14**, 635-643 (2006).
10. D. Sandler, "A multiple spot laser beacon for high-order wavefront control: theory and experiment", *Laser Guide Star Adaptive Optics Workshop*, Albuquerque, N.M.,R. Q. Fugate, Ed. 164-195 (1992).
11. D. G. Sandler, L. Cuellar, M. Lefebvre, T. Barrett, R. Arnold, P. Johnson, A. Rego, G. Smith, G. Taylor, and B. Spivey, "Shearing interferometry for laser-guide-star atmospheric correction at large D/r_o" *J. Opt. Soc. Am. A* **11**, 858-873 (1994).
12. E. Ribak and R. Ragazzoni, "Low power laser guide stars and wide field of view", *Proc. European Southern Observatory* **58**, 281-9 (2001).
13. Y. Baharav, E. N. Ribak, and J. Shamir, "Wide field analysis of turbulence layers using fringes in the mesosphere". *J. Opt. Soc. Am. A* **13**, 1083 (1996).
14. T. Berkefeld, D. Soltau, and O. von der Luhe, *Proc. SPIE* **4839,** 66-76 (2002).
15. E. N. Ribak, "Separating Atmospheric Layers in Adaptive Optics", *Opt. Lett.* **28**, 613-615 (2003).